Biomedical Signal Processing and Control 87 (2024) 105471

Contents lists available at ScienceDirect

Biomedical Signal Processing and Control

journal homepage: www.elsevier.com/locate/bspc

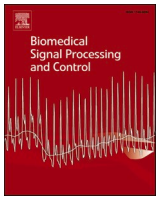

Comparison of filtering methods for real-time extraction of the volitional EMG component in electrically stimulated muscles

Matthew J. Hambly [a,b], Ana Carolina C. de Sousa [a,b,c], Claudio Pizzolato [a,b,*]

[a] Griffith Centre of Biomedical and Rehabilitation Engineering, Menzies Health Institute Queensland, Australia
[b] School of Health Sciences and Social Work, Griffith University, Queensland, Australia
[c] Research Centre for Biomedical Engineering at the Universitat Politècnica de Catalunya, Barcelona, Spain

ARTICLE INFO

Keywords:
Functional electrical stimulation (FES)
M-wave
Signal processing
Volitional electromyography (EMG)
EMG modelling
Motor unit recruitment

ABSTRACT

Objective: Recorded electromyograms (EMG) of electrically stimulated muscles can contain both an exogenous-evoked potential (M-wave) and an endogenous, or volitional, component. This study evaluated the effectiveness of three filtering methods (i.e., high-pass, adaptive, and comb), commonly used in neurorehabilitation, in extracting the volitional component of simulated and experimental EMG during upper-limb tasks.
Methods: Volitional EMG and M-wave were simulated through a physiological model of muscle recruitment, comprising of a motor neuron pool and associated muscle fibres, superimposed to a stimulation artefact. Experimental EMG data during different levels of volitional muscle contraction in isometric and dynamic tasks were recorded from five unimpaired individuals. Electrical stimulation artefact was removed with different techniques (i.e., none, removing samples, blanking, and interpolation) to assess filter performance across time and frequency domains, and information content (i.e., Kolmogorov-Smirnov D-value).
Results: The experimental results agreed with the simulations, wherein the adaptive filter outperformed the other filters when using no artefact removal or removing artefact samples from the signal, while for the blanking and interpolation artefact removal methods, the adaptive and comb filters outperformed the high-pass filter.
Conclusion: The adaptive and comb filters best estimated volitional muscle activity in electrically stimulated muscles.
Significance: Results from this study will enable the enhanced design of real-time neuroprosthesis control.

1. Introduction

Insult to the nervous system, such as a spinal cord injury or stroke, results in a partial or even complete loss of motor function, impacting the ability of an individual to volitionally activate their muscles [1]. Functional electrical stimulation (FES) is a widely used neurorehabilitation approach, whereby electrical pulses stimulate target muscles to elicit a contraction and generate movement. Stimulation parameters (i.e., pulse-width and amplitude) can be manually modified by the operator (e.g., clinician) or automatically by a control system and affect the level of muscle activation. When some motor function is retained following neural injury, it might be possible to boost the residual volitional muscle activity by using recorded electromyograms (EMG) as input to a control system, automatically initiating electrical stimulation of the same muscle [2]. Preliminary evidence suggested that enabling users to directly control their muscle stimulation may improve rehabilitation outcomes compared to non-EMG-based solutions [3–5]. However, EMG recordings of electrically stimulated muscles are contaminated by multiple sources and extracting the signal component associated with volitional muscle activation remains challenging.

The signal immediately recorded by surface EMG electrodes after muscle stimulation (i.e., 0 to 25 ms from first pulse) contains three main components: the volitional EMG (vEMG), the M-wave, and the stimulation artefact. The vEMG measures the electrical potential associated with muscle contraction generated via endogenous processes [6], providing information regarding the recruitment of motor neurons [7,8]. The M-wave represents the electrical potential associated with muscle contraction generated via exogenous processes and is the summation of the action potentials from the motor units being synchronously recruited by the electrical stimulus [6]. Finally, the stimulation artefact is the potential delivered by an electrical stimulation device to the muscle, which is an unwanted signal. During electrical stimulation of

* Corresponding author at: Griffith Centre of Biomedical and Rehabilitation Engineering, Menzies Health Institute Queensland, Australia.
E-mail address: c.pizzolato@griffith.edu.au (C. Pizzolato).

https://doi.org/10.1016/j.bspc.2023.105471
Received 6 January 2023; Received in revised form 22 August 2023; Accepted 12 September 2023
Available online 21 September 2023

muscles, these three signals partially overlap and must be appropriately filtered to enable vEMG or M-wave use in real-time neuroprosthesis control [9], and assessment of motor coordination and spasticity [10].

Several filtering methods have been proposed for real-time extraction of vEMG, M-wave, and stimulation artefacts. Stimulation artefacts have been successfully removed via software-based detection and removal techniques, showing low computational demand and a high success rate (i.e., >95 % of removed stimulation pulses) [11], eliminating the need for specialised hardware. Typical artefact removal methods include zeroing (i.e., blanking) the data [12–15], removing the samples from the signal entirely, or using interpolating splines [16,17]. High-pass filtering with a 200 Hz [15] or 330 Hz [18] cut-off frequency, adaptive filtering [19–21], and comb filtering with a fundamental frequency set equal to the stimulation frequency [13,22–24] are common methods used to extract vEMG during FES, but their performance has never been extensively compared. Previous work has qualitatively investigated differences between unfiltered and filtered signals in the time domain [22] or similarities in the frequency domain between the EMG signal without stimulation and with superimposed electrical stimulation after filtering [25], but without quantitative reporting. A range of metrics have also been used to assess the filtering performance, including signal to noise ratio between the filtered signal during stimulation with and without any volitional contributions [13], and reductions in the extracted vEMG signal power, coherence, and muscle response index following adaptive filtering [20]. Only one study has previously compared high-pass and adaptive filters, assessing their ability to extract vEMG for different levels of stimulation [14]. Moreover, previous work assessed the filter performance using simulated data [20,21] or only in either isometric [13,25] or dynamic [14,22] experimental conditions. As such, it remains unclear what filter best retains the information characteristics of the extracted vEMG signal across both isometric and dynamic conditions.

This study assessed three of the most used methods to extract vEMG during FES: high-pass, adaptive, and comb filters. Our aim was to evaluate each filter's performance combined with artefact removal, using first simulated EMG data and then experimental EMG recordings across isometric and dynamic upper-limb motor tasks. Performance was assessed in time and frequency domains by evaluating the similarity of the information content between EMG in the absence of stimulation and vEMG extracted by each of the filters during superimposed electrical stimulation. The potential time delay introduced by each M-wave filter was also considered to evaluate real-time suitability.

2. Method

2.1. Simulation of EMG data

The performance of the proposed filters was first evaluated using simulated EMG data. To this end, we developed a physiological model of a motor neuron pool and associated muscle fibres combined with a model simulating the impedance of muscle, fat, skin, and electrodes [26,27] (Fig. 1). Our approach allowed the simulation of vEMG as well as M-wave following exogenous electrical stimulation [28]. Motor neurons were implemented using a leaky fire-and-integrate model [29]. Physiological firing behaviour of the motor neuron pool was achieved by controlling the common synaptic current to the motor neuron pool [30] and via the appropriate selection of neurons' electrical characteristics [31]. Motor units were modelled by connecting each motor neuron to multiple muscle fibres, using parameters obtained from the literature [27,28,30,32] and reported in Table 1. Each muscle fibre intracellular action potential was generated at the neuromusculoskeletal junction as a function of motor neuron firing, and described by the following equation [33]:

$$V_m(z) = \begin{cases} Az^3 e^{-z} + B, & z > 0 \\ 0, & z \leq 0 \end{cases}, \quad (1)$$

where $A = 96mV.mm^{-3}$, $B = -90mV$, and z is the spatial direction along the muscle fibres.

Action potentials were modelled to propagate along the length of the muscle fibres at constant velocity (Table 1) and to extinct at the tendon. Muscle fibres were spatially located within a cylinder of radius 21 mm (calculated from the cross-sectional area of the biceps brachii [34]) following a uniform distribution. The transfer function between the current density source within the muscle fibre and bipolar circular electrodes positioned on the skin accounted for the physical characteristics of the electrode detection system, including electrode shape and interelectrode distance, and the volume conductor properties of the skin, fat, and muscle layers [26]. The potential difference of each muscle fibre

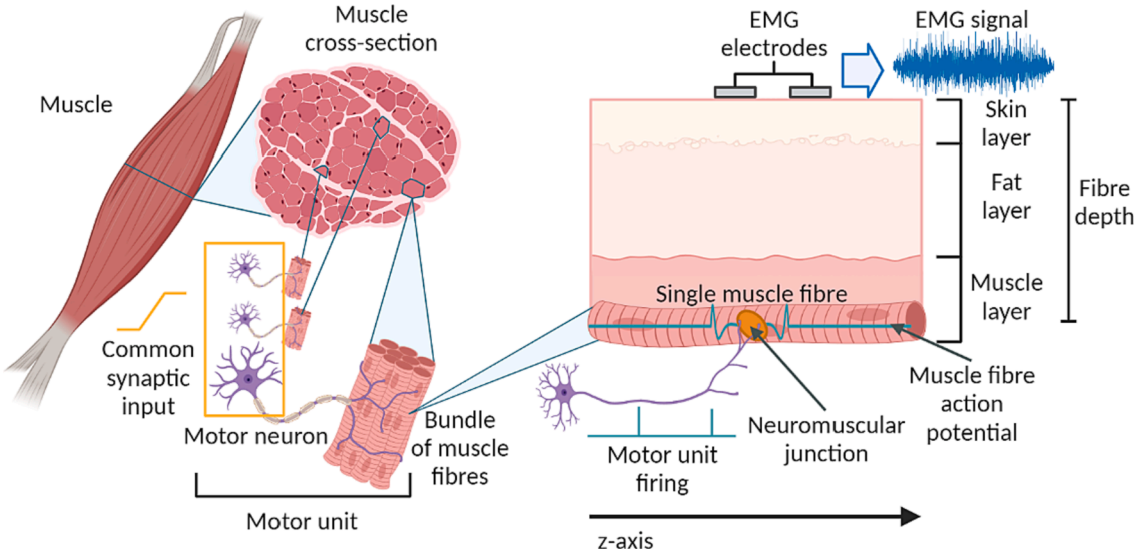

Fig. 1. Representation of the physiological elements included in the computational model for EMG simulation. Each motor unit comprised of a motor neuron innervating multiple muscle fibres. The common synaptic input current was provided to all neurons within the motor neuron pool, enabling orderly recruitment consistent with Henneman's size principle [31]. Action potential was initiated at the neuromuscular junction of each muscle fibre as a function of motor neuron firing, propagating along the length of the fibre (z-axis). For each electrode, EMG potential at the skin level was modelled via a transfer function accounting for skin, fat, and muscle layers, and subtracted to simulate the bipolar configuration.

Table 1
EMG simulation parameters used throughout the current study.

Parameter	Value
Muscle radius	21 mm [34]
Number of motor units	65 [28]
Number of muscle fibres *(uniform distribution)*	50 – 450 [28]
Muscle fibre length *(normal distribution)*	130 (±3) mm [28]
Neuromuscular junction location *(normal distribution)*	0 (±1) mm from centre [32]
Conduction velocity *(normal distribution)*	4 (±0.3) m/s [28]
Neuron resistance *(uniform distribution)*	0.5e6 – 4.1e6 Ω [30]
Sampling frequency	2000 Hz
Electrode radius	12.5 mm
Interelectrode distance	20 mm
Angle of inclination	0°
Thickness of fat layer	3 mm [26,27]
Thickness of skin layer	1 mm [26,27]
Fat conductivity	0.05 S/m [27]
Skin conductivity	1 S/m [27]
Muscle conductivity longitudinal to fibre direction	0.5 S/m [27]
Muscle conductivity transversal to fibre direction	0.1 S/m [27]

was calculated between two points on the skin surface along the fibre axis, representing a bipolar configuration of electrodes with an inter-electrode distance of 20 mm, placed at the centre of the muscle along the direction of the fibres. The compounded sum of these simulated measurements across all muscle fibres resulted in the generation of time-varying EMG data (Fig. 2). To simulate an M-wave, action potentials were synchronously generated across a percentage of muscle fibres selected as a function of the stimulation current.

All simulations were conducted using a bipolar circular electrode configuration. To simulate vEMG, the common synaptic current to the motor neuron pool was set as a percentage (20 %, 40 %, 60 %, and 80 %) of the maximum input current (25 nA). To simulate the M-wave, a group of motor units were all activated synchronously at a stimulation frequency of 25 Hz, with the number of motor units being a percentage (20 %, 40 %, 60 %, and 80 %) of the total motor units proportional to the desired level of stimulation (Fig. 2 (b)). The specific portion of motor units that were recruited at each stimulation level were selected in order of increasing conduction velocity and depth [28]. The stimulation level remained constant for the entire 2 s simulation for each increment. Each of the four vEMG and four M-wave trial conditions were then combined by summing the two signals together at each time point to create the M-wave contaminated vEMG signal, generating 16 trials in total. Additionally, a vEMG signal with 100 % of the maximum neural input was generated as the maximum volitional contraction (MVC) for normalisation in the processing steps. The stimulation artefact, which is present when recording experimental EMG during electrical stimulation, was modelled as a biphasic square pulse wave (each phase 500 μs wide) and added to the simulated EMG signals synchronously with the recruitment of motor units, using an amplitude of the pulse four times larger than the MVC [16].

2.2. Experimental data collection protocol

A testing protocol was developed incorporating both isometric and dynamic biceps brachii contraction conditions, comprising different levels of electrical stimulation and volitional muscle activation. Five unimpaired participants (age 26.8 ± 3.6 years, body mass 78.2 ± 14.5 kg, height 1.75 ± 0.06 m) took part in this study, and each provided informed consent. The Griffith University Human Research Ethics Committee approved the study (GU ethics no: 2021/298).

For each participant, a single arm was prepared for data collection. Surface EMG of the biceps brachii was recorded at 2000 Hz (Atkos, Myon, Switzerland), with the site cleaned, prepared and Ag/AgCl bipolar electrodes, having a 12.5 mm radius and 20 mm inter-electrode distance (Duotrode, Myotronics, USA) placed according to SENIAM guidelines [35]. Circular FES electrode pads with a radius of 16 mm (PALS Platinum, Axelgaard, USA) were placed proximally and distally to the EMG electrodes (Fig. 3(a)), following manufacturer guidelines [36], and connected to a programmable FES system (Rehastim2, Hasomed, Germany). The muscle's MVC for each participant was identified at the beginning of each session by flexing the elbow to push maximally against a fixed resistance for 3 s, with three valid trials recorded, allowing for 30 s of rest between trials. The participants' maximum stimulation current level was obtained via an iterative process, whereby the muscle was stimulated with the maximum pulse-width of 500 μs and increasing the current amplitude in steps of 2 mA. At each step, the participant was asked to assess their discomfort level and verbally confirm whether they desired to continue increasing the stimulation

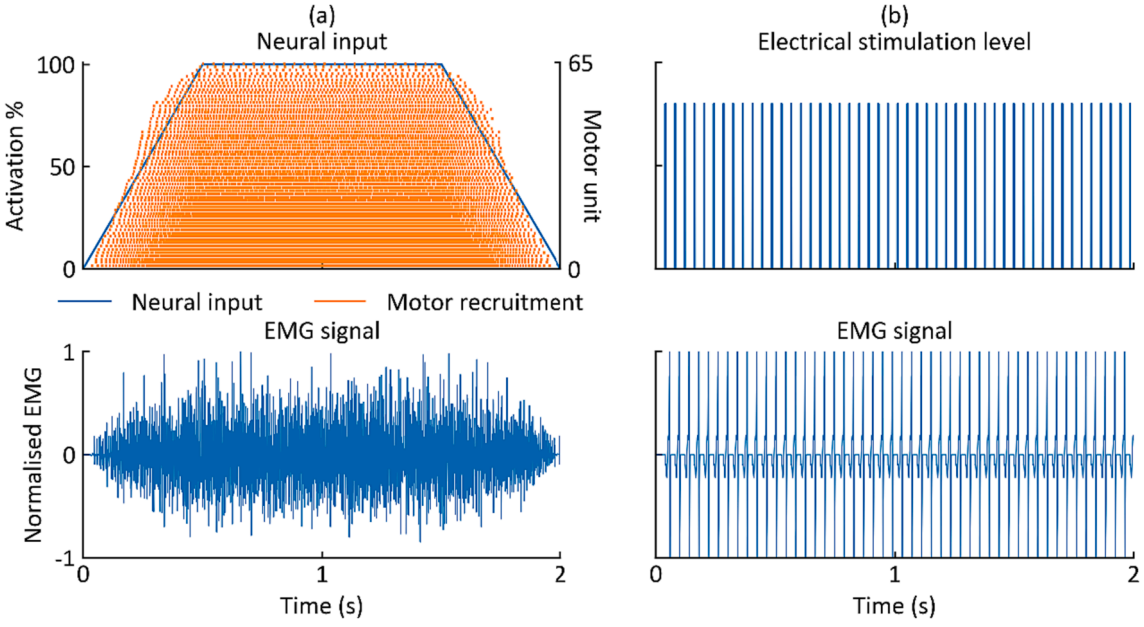

Fig. 2. Example of the simulation of (a) volitional and (b) evoked EMG signals. For the vEMG, a neural input current is ramped from zero to the maximum, resulting in an increasing number of motor units firing and an increasing amplitude of generated vEMG signal. For the evoked activations, the motor units were recruited at the stimulation frequency (25 Hz), producing a synchronous M-wave.

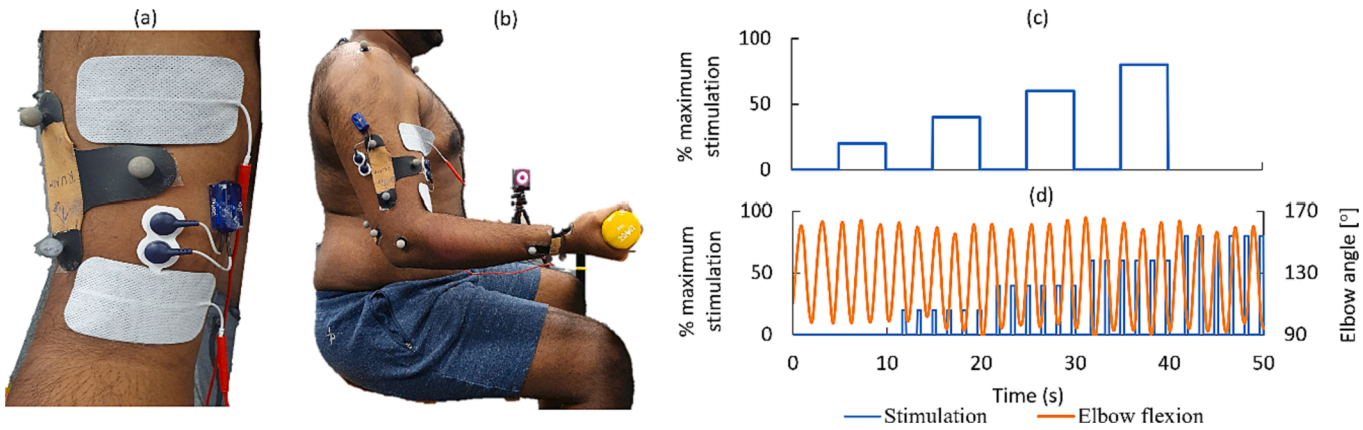

Fig. 3. (a) Placement of the EMG and FES electrodes on the biceps brachii. (b) Participant seated with the elbow flexed at 90°. (c) Stimulation pattern for the isometric task. (d) Stimulation pattern and elbow flexion angle for the dynamic task.

level. The maximum current for the participant was selected to be the one below the self-perceived level of discomfort. The pulse-width and maximum current then informed the maximum stimulation charge applied to the muscle for each participant. The mean maximum stimulation current across the participants was 11.2 ± 2.3 mA. A stimulation frequency of 25 Hz was used throughout the experimental protocol. Motion capture data were recorded at 200 Hz using a Vicon 12-camera (MX T40-S) motion capture system (Vicon Motion Systems, Oxford, UK). Eight retroreflective markers were placed on the torso and arm to track their 3D motion. The recorded motion data was used to split the dynamic trials into individual elbow flexion and extension cycles during the processing.

The isometric tasks required the participants to sit flexing their elbow at 90°, lower arm supinated, and shoulder held at 0° in all degrees of freedom (Fig. 3(b)), maintain a constant elbow angle throughout the trial, and hold a series of weights (1 kg, 3 kg, and 5 kg) or no weight. Each trial consisted of four 5 s repetitions without stimulation followed by 5 s with stimulation of the biceps brachii, with the stimulation charge starting at 20 % of the maximum stimulation charge previously identified for the participant and reaching 80 %, incrementing by 20 % (Fig. 3 (c)). The participant was instructed to maintain an elbow angle of 90° for the entire trial, which was visually monitored to maintain consistency.

The dynamic tasks required the participant to flex and extend their elbow at a frequency of 0.5 Hz for 50 s, while the lower arm remained supinated (Fig. 3(d)). In the first 10 s of each trial, no stimulation was provided. Then, for the remaining 40 s, the biceps brachii was stimulated for a duration of 0.4 s every 1.6 s. A digital metronome operating at 0.5 Hz was used to provide auditory feedback to the participants to assist with their timing and standardise the movements across trials. By offsetting the stimulation delivery and flexion cycle frequencies, the muscle was stimulated during different stages of activation, increasing the conditions to evaluate across. The stimulation charge was then incremented by 20 % of the maximum electrical stimulation charge for the participant every 10 s, starting at a baseline of 20 % and reaching 80 % (Fig. 3(d)).

Each participant performed one trial per weight condition for both the isometric and dynamic tasks, with 60 s of rest between trials, starting with no weight and then consistently increasing within the series (1 kg, 3 kg, and 5 kg).

2.3. Data processing

Marker data were labelled and gap filled in Vicon Nexus (Vicon Nexus 2.12, Oxford, UK) and exported into OpenSim (Version 4.1) [37]. A generic arm model [38] was scaled to each individual using markers positioned on the acromion process, lateral elbow condyle, and ulnar styloid process. Inverse kinematics was used to calculate the elbow angle for all dynamic trials and automatically segment the trials into individual elbow flexion–extension cycles, automatically identified via a peak finding method. The dynamic trials were divided into smaller segments of 2 s containing a single full elbow flexion and extension cycle and a different time region stimulated in each segment, producing between 4 and 5 segments per trial depending on the timing of the movement.

An offline EMG filtering pipeline was developed in MATLAB (2022b) to remove stimulation artefact and M-wave to extract the vEMG for evaluating the different filtering methods (Fig. 4). The pipeline first implemented a custom software-based artefact detection algorithm to identify and remove the regions contaminated by stimulation artefact. Similar to [11], the artefact detection method used mean and standard deviation of the EMG second derivative to identify artefacts, but the adaptive tuning parameter and buffering were removed to better suit suitable real-time applications. Here, mean and standard deviation were calculated using the entire data length, while in real-time the cumulative mean and standard deviation may be used. The thresholds used to identify the artefact were calculated as

$$th_{upper} = \overline{\frac{d^2x}{dt^2}} + \sigma, \tag{2}$$

$$th_{lower} = \overline{\frac{d^2x}{dt^2}} - \sigma, \tag{3}$$

where th_{upper} and th_{lower} are the upper and lower thresholds, respectively, $\overline{\frac{d^2x}{dt^2}}$ is the mean of the second derivative of the EMG signal and σ is the standard deviation of the EMG second derivative. The signal derivatives were calculated using backward numerical differentiation. If the amplitude of the second derivative of the input signal was greater than the upper threshold (th_{upper}) or less than the lower threshold (th_{lower}), the sample was marked as a stimulation artefact. A limit was introduced to restrict the potential for false artefact detection so that no artefact could be detected less than half a stimulation period after the previous. The artefact region length was related to the stimulation pulse-width and a tuning parameter n, represented by the equation

$$l_{artefact} = n \cdot pw, \tag{4}$$

where $l_{artefact}$ is the artefact region, and pw is the stimulation pulse-width [16]. The value used for the tuning parameter n should lie within the range 12–20 [16], with a value of 16 used here based on initial testing that evaluated the root mean squared error (RMSE) and Pearson's coefficient of determination (R^2) between EMG with no stimulation and the EMG during stimulation after the artefact was removed with n values ranging from 1 to 50. Multiplying the artefact

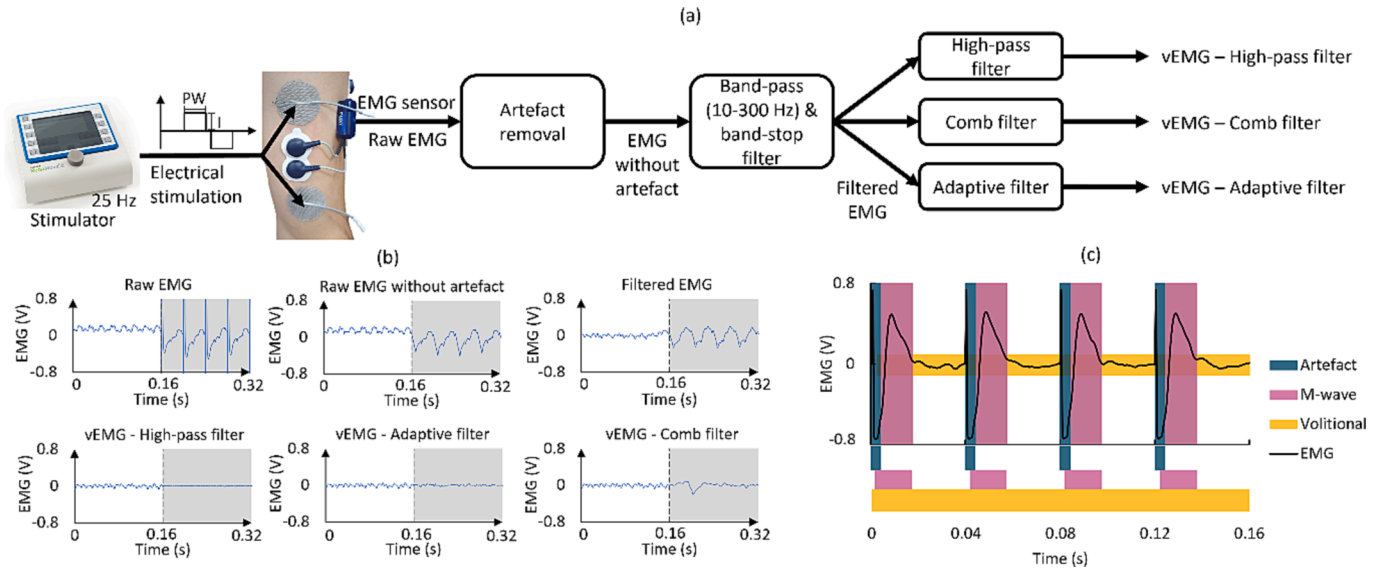

Fig. 4. (a) EMG signal processing procedure to extract the vEMG. Pulse-width (PW) and current amplitude (I) values were provided to stimulate the biceps brachii, while EMG activity was recorded. Stimulation artefact was then detected, and the samples were either unchanged, removed from the signal, replaced with zeros or interpolation. The proceeding processing steps were then completed separately on each of these four artefact removal methods. The signal was then band-pass and band-stop filtered. Finally, the volitional component of the EMG was extracted using high-pass, adaptive and comb filters. (b) The output EMG signals from each processing step under isometric conditions, with the shaded areas representing the time that stimulation was applied, with the output after the interpolation artefact method used as an example here. (c) An example of a raw surface EMG signal containing the stimulation artefact, M-wave, and volitional muscle activity.

region gain by the pulse-width allows for the region to be fully encapsulated and removed at all stimulation charge levels while retaining as much of the original signal as possible at the lower pulse-width values where the stimulation artefact may not last as long as the higher charge values. For a comprehensive comparison, four separate output signals were obtained from the artefact detection: taking no action on the region, removing the region entirely, replacing the region with zeroes (i.e., blanking) [12–15,21] or replacing the region with interpolation [16,17]. After removing the stimulation artefact, the signal was band-pass filtered between 10 and 300 Hz, and band-stop notch filtered at 50 Hz using 3rd order Butterworth filters forwards and backwards in time (see [14] for filter design), removing noise and amplitude offset. Cut-off frequencies of 10 and 300 Hz were chosen for the band-pass filter as most vEMG spectral energy typically occurs within this range [14,39], while 50 Hz was used for the band-stop notch filter to remove powerline noise [40], with cut-off frequencies of 49 Hz and 51 Hz used to create a narrow notch centred at 50 Hz [41]. When stimulation was active, the EMG signal was separately passed through each filter being assessed, a high-pass [15], an adaptive [21], and a comb filter [13]; when the stimulation was inactive, no further processing was performed. These three filters were chosen for evaluation due to their relatively common use in previous studies.

The high-pass filter was a 6th order elliptic filter with a cut-off frequency of 200 Hz, 3 dB of ripple in the passband and 80 dB of attenuation in the stopband, applied forwards and backwards in time. High-pass filtering has been used in previous studies to attenuate low frequencies associated with the M-wave. The comb filter had a fundamental frequency the same as the stimulation frequency (25 Hz), represented by the difference equation

$$y(i) = \frac{x(i) - x(i-T)}{\sqrt{2}}, \tag{5}$$

where $y(i)$ is the filtered EMG signal, $x(i)$ is the input EMG signal, and T is the number of samples in one stimulation period, which can be calculated as

$$T = \frac{f_{emg}}{f_{stim}}, \tag{6}$$

where f_{emg} is the EMG sampling frequency and f_{stim} is the stimulation frequency. This type of comb filter minimises the noise introduced by the stimulation at the stimulation period and its harmonics through the repeating notch filter nature of the comb filter. Finally, the adaptive filter used EMG samples from the previous six stimulation periods to estimate the stationary noise, including the M-wave, which was then subtracted from the current EMG signal, as represented by the equation

$$y(i) = x(i) - \sum_{j=1}^{M} b_j x(i - jT), \tag{7}$$

where $y(i)$ is the filtered EMG signal, $x(i)$ is the input EMG signal, M is the number of previous stimulation periods used for the estimation (here $M = 6$), b_j are the filter coefficients for each frame adapted at the stimulation frequency, and T is the number of samples in one stimulation period. For each new stimulation period, the optimal filtering coefficients were recalculated using a least square algorithm minimising the energy output of the current frame with respect to the filter coefficients to predict the stationary component of the signal considered as noise, importantly including the M-wave here, and subtracted from the EMG signal [21] (Fig. 5). When artefact samples were removed entirely, f_{emg} (equation (6)) for both the comb and adaptive filters was recalculated considering the samples removed from the period. The high-pass and adaptive filters required a window of EMG samples to effectively perform filtering, therefore, the EMG signal was buffered to contain one stimulation period before passing through these two filters, with the previous six buffers stored in memory for use in the adaptive filter. The frequency response of the three M-wave filtering techniques was displayed in Fig. 6, with an example of the adaptive filter frequency response obtained using the filter coefficients while filtering out M-wave during an isometric trial at different intervals (25 %, 50 %, 75 % and 100 %) of the trial time.

The filtered signals' linear envelope and Fast Fourier transform were obtained for subsequent performance analyses. The linear envelope was calculated via rectification and low-pass filtering using a 4th order zero-lag Butterworth filter with a cut-off frequency of 5 Hz [24,42]. The signals were normalised to the participant-specific MVC, using a MATLAB script to identify peak values across all MVC trials.

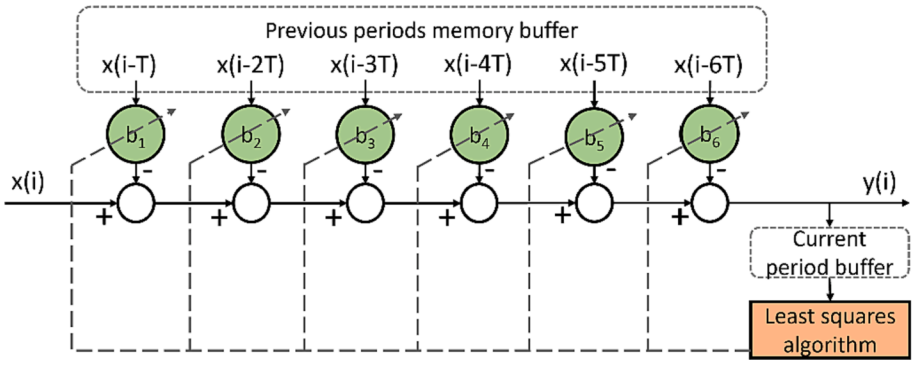

Fig. 5. Schematic of the operation of the adaptive filter used in this study. A memory buffer stores the samples from the previous six stimulation periods (T) and multiplied by the corresponding filter coefficient (b), to represent stationary noise, and then subtracted from the current samples (x) to obtain the filtered signal (y). A least squares algorithm is used to adapt the filter coefficients at each stimulation period using the samples from the current stimulation period.

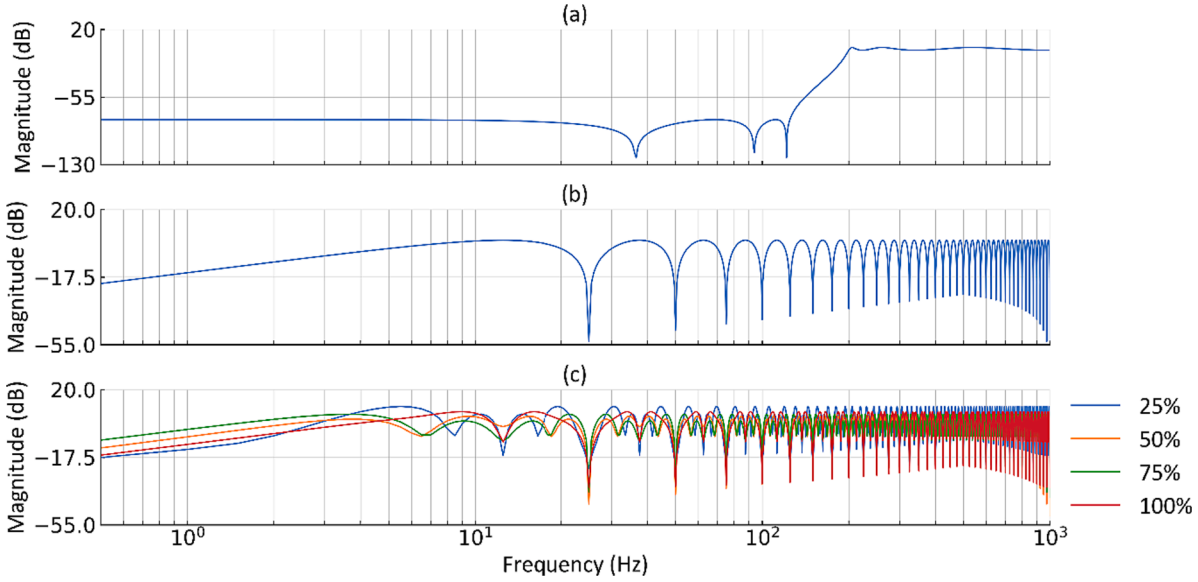

Fig. 6. Frequency response of the (a) high-pass, (b) comb and (c) adaptive filters. The frequency response was calculated using frequencies up to the Nyquist frequency of 1000 Hz. As the frequency response of the adaptive filter changes with the update of coefficients, an example response at different time intervals (25 %, 50 %, 75 % and 100 % of the maximum trial time) of a single M-wave filtering trial is displayed.

2.4. Performance analysis

For each filter and artefact removal method combination, the extracted vEMG was compared to the corresponding EMG data in the absence of stimulation. Filtering performance was assessed via three outcome measures applied to each trial: RMSE, R^2, and the Kolmogorov-Smirnov statistic (D-value). RMSE was calculated between the time series envelopes of the baseline and filtered signals to assess time domain similarities. R^2 was calculated between the frequency spectrum of the baseline EMG signal and the extracted vEMG signals, assessing the similarities in the frequency domain. The D-value compared the information content of EMG and extracted vEMG signals and was calculated via a Kolmogorov-Smirnov test [43]. The probability density function (PDF) of each non-enveloped time domain signal was determined, and the empirical cumulative density function (eCDF) was found from the PDF. The D-value was calculated as the maximum difference between the eCDF of the baseline EMG and the extracted vEMG signals. A larger D-value suggests a greater difference between the information content of the two signals and, therefore, worse performance for the filter.

2.5. Statistical analyses

We combined performance metrics for all trials across weight and stimulation conditions for the simulated and experimental data to identify the best filter within each artefact removal method. As the data were not normally distributed, according to a Shapiro-Wilk test [44], a Kruskal-Wallis analysis of variance (ANOVA) test was used to determine significant differences between the filtering methods within each artefact removal technique and performance metric, with significance set to $p < 0.05$.

3. Results

A total of 16 simulated trials of length 2 s, 80 experimental isometric trials of length 5 s, and 348 dynamic trials of length 2 s per trial were recorded. Typical examples of data were reported for visual inspection, including raw and filtered simulated and experimental EMG data (Fig. 7), as well as normalised linear envelopes (Fig. 8(a)), frequency spectrums (Fig. 8(b)), and D-values from the PDF (Fig. 9(a)) and eCDF (Fig. 9(b)) for the dynamic elbow flexion–extension.

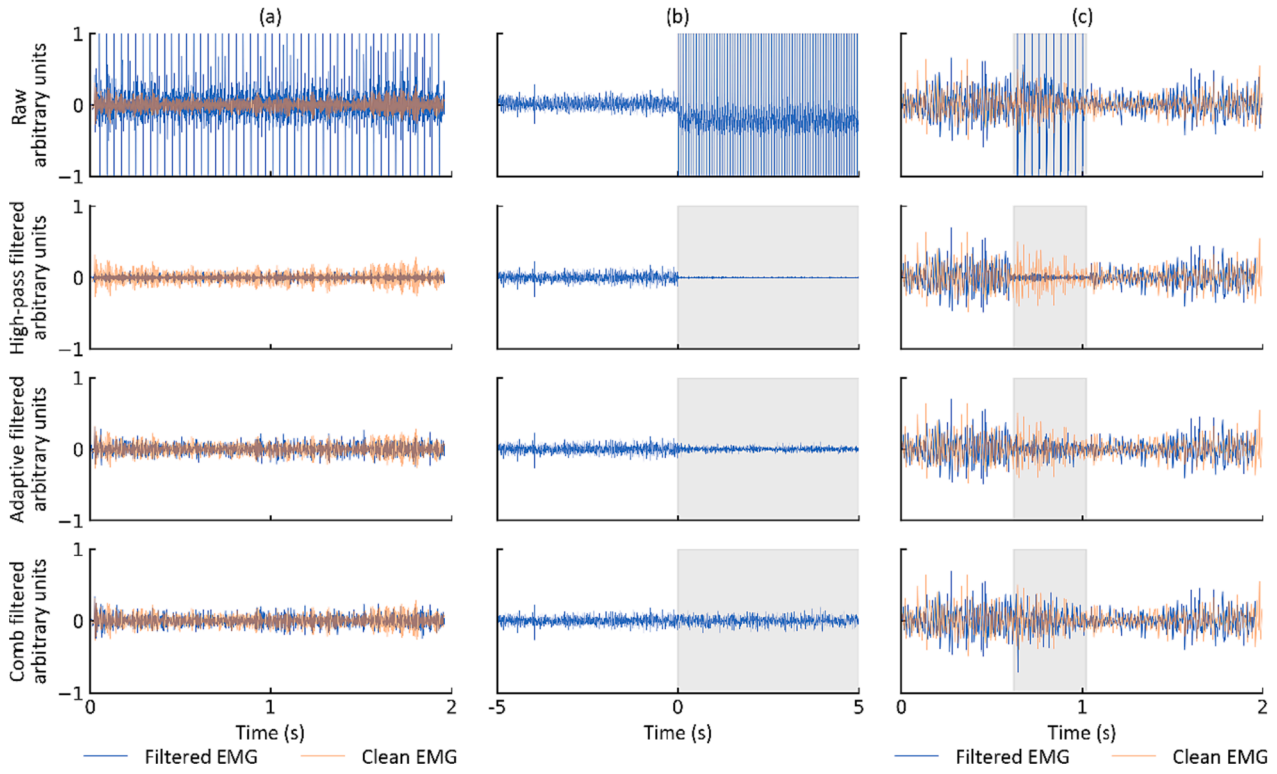

Fig. 7. Examples of the raw and filtered EMG signals (high-pass, adaptive and comb filtered) to be used in the analysis from the (a) simulated data with 80 % stimulation and 60 % maximum volitional activation, and experimental data from participant one with 80 % stimulation and 3 kg weight during the (b) isometric elbow task and (c) one of the elbow flexion and extension cycles of the dynamic task trial. The grey shaded areas in (b) and (c) represent the periods where stimulation is active and vEMG extraction occurs. For the dynamic task, multiple flexion and extension cycles are recorded with the region that stimulation is active being different for each cycle.

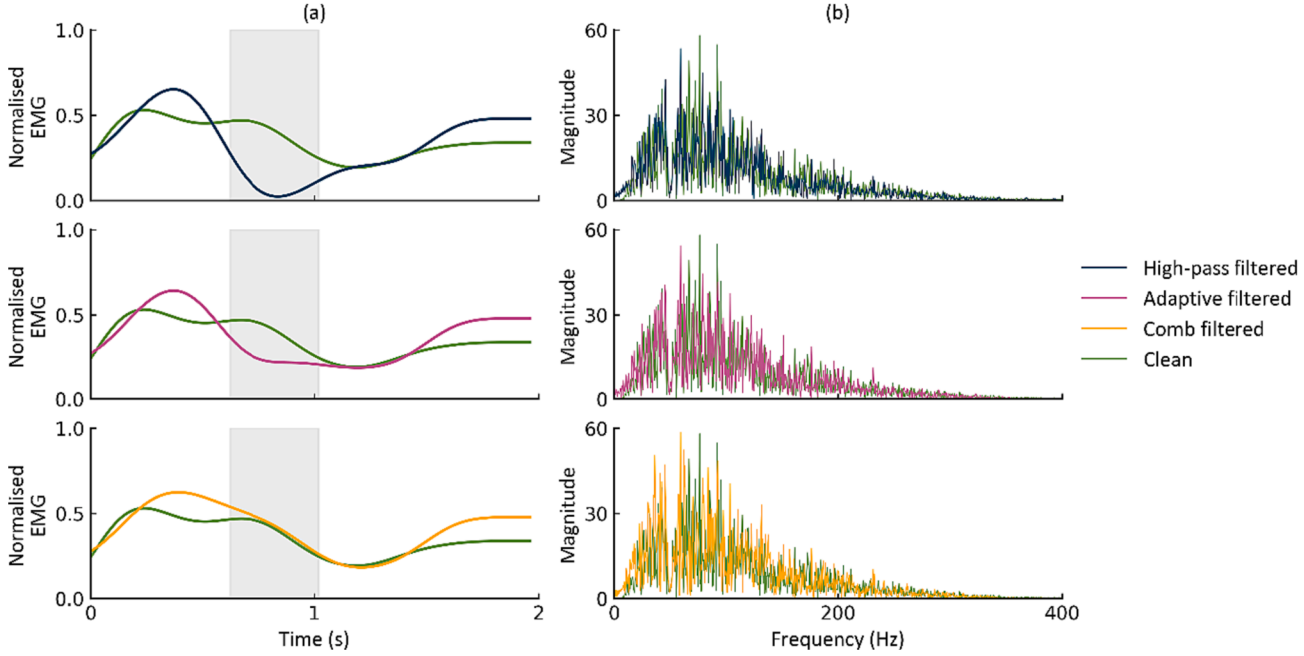

Fig. 8. The EMG without any stimulation (clean) and the extracted vEMG signals from each of the three filters (high-pass, adaptive and comb) during one extension and flexion cycle from participant one with 80 % stimulation and 3 kg weight during the dynamic elbow task represented by (a) the linear envelope for the calculation of the RMSE and (b) the frequency domain for calculation of R^2. The shaded grey area represents active stimulation, and the three filters were applied.

3.1. Simulation results

For the simulated data (including stimulation artefact), the adaptive and comb filters produced significantly lower RMSE than the high-pass filter (Fig. 10(a)). The high-pass filter also provided R^2 and D-value metrics significantly lower and significantly higher, respectively, than

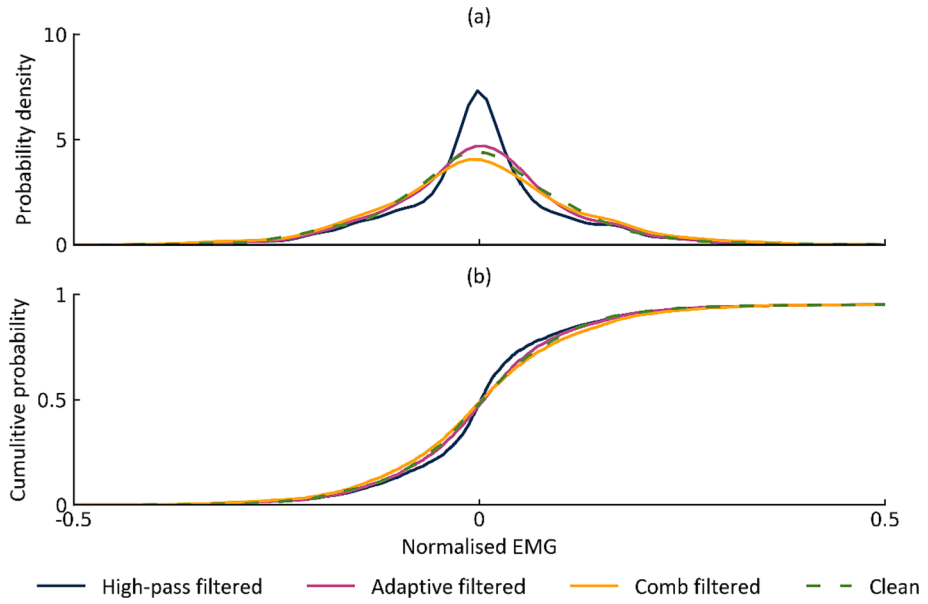

Fig. 9. The EMG without any stimulation (clean) and the extracted vEMG signals displayed as their (a) PDF and (b) eCDF to calculate the D-value during one extension and flexion cycle from participant one with 80 % stimulation and 3 kg weight during the dynamic elbow task.

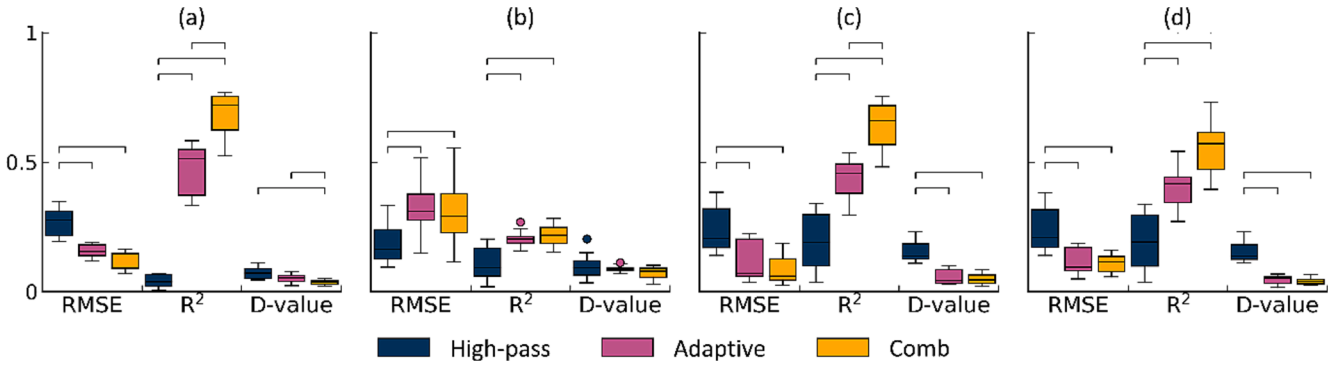

Fig. 10. Box plots from simulated EMG data for the performance of the high-pass, adaptive and comb filters, with (a) no artefact removal, (b) removing the samples entirely, (c) blanking the samples and (d) linear interpolation. Data was combined across all volitional muscle activation and stimulation conditions. The horizontal bars represent a significant difference ($p < 0.05$) between filters.

the other filters (Fig. 10(a)). When the artefact-contaminated samples were removed from the signal, the adaptive and comb filter produced significantly higher RMSE than the high-pass filter, while the high-pass filter produced significantly lower R^2 than the other filters (Fig. 10(b)). For both the artefact blanking and interpolation methods, the adaptive and comb filters produced significantly lower RMSE and D-value and higher R^2 than the high-pass filter (Fig. 10(c–d)). The comb filter also provided a significantly higher R^2 than the adaptive filter when blanking or using linear interpolation (Fig. 10 (c–d)).

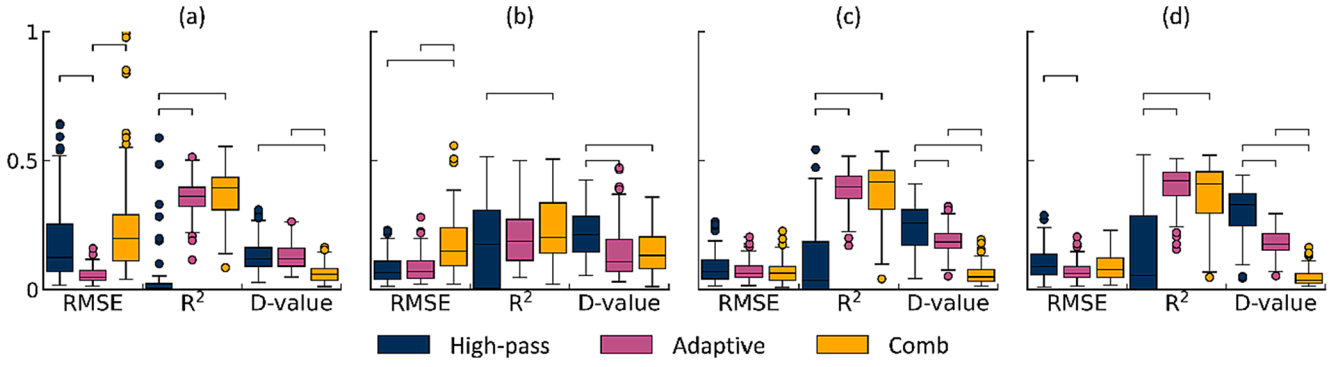

Fig. 11. Box plots from the isometric flexion experimental EMG data for the performance of the high-pass, adaptive and comb filters, with (a) no artefact removal, (b) removing the samples entirely, (c) blanking the samples and (d) linear interpolation. Data was combined across all volitional muscle activation and stimulation conditions. The horizontal bars represent a significant difference ($p < 0.05$) between filters.

3.2. Experimental results

In isometric conditions, when not using any artefact removal, the adaptive filter showed significantly lower RMSE than the other filters, and significantly higher R^2 than the high-pass filter. In contrast, the comb filter showed a significantly lower D-value than the high-pass and adaptive filters (Fig. 11(a)). When removing the artefact samples from the signal the high-pass and adaptive filters provided significantly lower RMSE than the comb filter, while the high-pass filter provided significantly lower R^2 than the comb filter, and significantly higher D-value than both other filters (Fig. 11(b)). For the blanking method, the adaptive and comb filters both produced significantly greater R^2 than the high-pass filter, while the comb filter produced a significantly lower D-value than both other filters (Fig. 11(c)). Similarly with the interpolation removal strategy, both the adaptive and comb filters provided significantly higher R^2 than the high-pass filter, and the comb filter provided significantly lower D-value than the other filters, while the adaptive filter provided significantly lower RMSE than the high-pass filter (Fig. 11(d)).

In dynamic conditions, when not using any artefact removal, the adaptive filter showed significantly lower RMSE and D-value than the high-pass and comb filters, while the adaptive and comb filters both produced significantly higher R^2 than the high-pass filter (Fig. 12(a)). When removing the artefact samples entirely, the comb filter provided significantly higher RMSE and lower R^2 than the high-pass and adaptive filters, however it also provided significantly lower D-value than the other filters (Fig. 12(b)). For the blanking method, the adaptive filter produced a significantly lower RMSE than the other filters, a significantly higher R^2 than the comb filter, and both the adaptive and comb filters produced a lower D-value than the high-pass filter (Fig. 12(c)). The interpolation method also produced similar results, with the adaptive filter providing significantly lower RMSE and D-value than the other two filters, while the high-pass and adaptive filters produced higher R^2 than the comb (Fig. 12(d)).

4. Discussion

We implemented and compared three filtering methods to extract vEMG during electrical stimulation of muscles. We developed a computational model of EMG generation driven by physiological muscle recruitment, which enabled the simulation of both vEMG and M-wave. The simulation results were then extended via in vivo testing across a range of muscle activation levels and electrical stimulation intensity. The adaptive and comb filters best performed across all conditions and performance metrics, suggesting they should be preferred when extracting vEMG signals during electrical stimulation of muscles.

We developed a physiological computational model for generating vEMG and M-wave of electrically stimulated muscles. Specifically, a previously validated model of orderly motor neuron recruitment from a common synaptic current to the motor neuron pool [30] was combined with a validated model of EMG generation from intracellular muscle fibre action potential [26], enabling the exploration of filtering approaches across different levels of muscle activation and electrical stimulation. Simulated vEMG data represented the ground truth, which was subsequently contaminated with M-wave and stimulation artefact, thus enabling faithful evaluation of filter performance. The simulated results demonstrated that overall, the adaptive and comb filters provided the best vEMG estimates, other than the RMSE, when artefact samples were removed from the signal (Fig. 10). However, this strategy distorts the sampling frequency depending on the artefact detection and stimulation timing, requiring recalculation of all filter coefficients as a function of the number of removed samples. These results confirm those of previous simulation studies, which used an exponentially damped sinusoid to represent the M-wave combined with either additive band-limited Gaussian noise to represent the volitional activity [21] or experimental vEMG data [20]. Critically, the ability of our computational model to simulate EMG using a physiological motor neuron recruitment strategy, accounting for the number and characteristics of motor units, and tuneable to accommodate soft tissue variations (e.g., skin and fat thickness, muscle size) has the unique potential to enable exploring the effect of filtering during FES in a variety of populations and conditions (e.g., alteration in recruitment following neural injury, muscle atrophy), beyond the analyses presented in this study.

The results of our in silico experiments were verified in vivo, confirming the performance of comb and adaptive filters. For both isometric and dynamic tasks, the adaptive filter was typically the best performing when used with the raw signal (i.e., no artefact removal), while the comb and adaptive filters best performed with artefact blanking and interpolation strategies (Fig. 11 and Fig. 12). Overall for all artefact removal techniques, and in agreement with our simulated data, the high-pass filter was the worst performer due to the removal of a significant amount of information from the vEMG signal typically occurring between 30 and 300 Hz [39] (Fig. 6). Our results extended previous studies showing improvement in the comb filter performance for extracting vEMG when including stimulation artefact blanking [13], the ability of adaptive filtering to removing the M-wave during dynamic movements [21], and overall improved vEMG during electrical stimulation compared to high-pass filtering [14]. Conversely, our comprehensive assessment did not support previous investigations showing that high-pass filtering could perform well in extracting vEMG from contaminated signals [15].

Real-time vEMG can be used as feedback to improve existing rehabilitation paradigms [3–5] and enhance neurally connected neuroprostheses that combine stimulation and robotic assistance [9,45,46]. Critically, these applications require real-time processing of the acquired EMG signal with minimal time delay. While in this study all

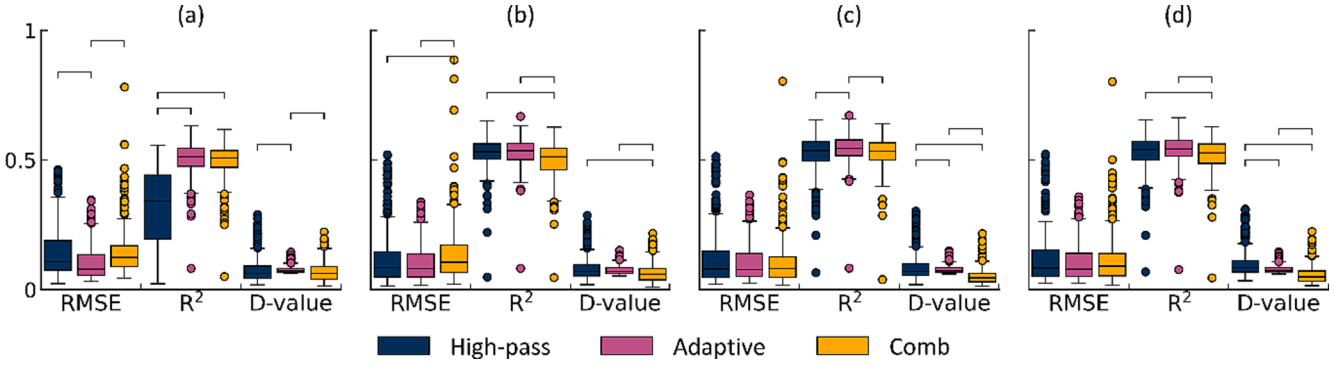

Fig. 12. Box plots from the dynamic flexion experimental EMG data for the performance of the high-pass, adaptive and comb filters, with (a) no artefact removal, (b) removing the samples entirely, (c) blanking the samples and (d) linear interpolation. Data was combined across all volitional muscle activation and stimulation conditions. The horizontal bars represent a significant difference ($p < 0.05$) between filters.

processing steps were performed offline, these same algorithms have been previously used in real-time [11,23]. Both the implemented high-pass and adaptive filters required buffering of the EMG signal to operate effectively, introducing a delay of up to one stimulation period (i.e., 40 ms for 25 Hz stimulation), while the comb filter could be performed without any buffering, only requiring data from the latest EMG sample up until one stimulation period prior. A shorter buffer length could be used for the high-pass filter to reduce delay; however, the adaptive filter requires the buffer length to be a ratio of the EMG sampling frequency to the stimulation frequency (i.e., the number of samples in a stimulation period) so that the M-wave of each frame is aligned with previous stimulation period frames for removal [21]. The comb filter relied on samples up until one stimulation period before the current sample and, therefore, cannot filter data received during the first stimulation period. However, this would not affect real-time suitability. Additionally, the evaluated comb filter is a causal finite impulse response filter [13] with a delay equivalent to half the stimulation period [47,48]; however, this delay is less than the delay introduced by the buffering required for the high-pass and adaptive filtering methods. These time delays are unlikely to interfere with FES control systems, which operate at the same frequency of stimulation; however, applications involving robotic assistance [49] and biofeedback [50] are time critical and should be optimised for minimal delays. Consequently, time-sensitive applications should prefer a comb filter over other evaluated approaches. Finally, our data analyses employed non-causal bidirectional band-pass and band-stop filters for signal preconditioning prior to M-wave removal. For real-time applications, these filters should be replaced with their causal equivalent applied forwards in time only, with the filter order doubled to account for the change to unidirectional operation. A trade-off between filter order and time delay should also be considered [51,52].

Additional artefact removal methods and filters that could further improve outcomes do exist, but were not assessed, as not commonly used in FES applications. Software-based artefact removal approaches reduce the dependence on specialised hardware for synchronisation or blanking with specific circuitry, increasing the adaptability of the approach to potentially be more easily used with a large variety of setups. Linear interpolation was selected as a simple alternative to the commonly used blanking method following reports of improved performance [16], yet it might be susceptible to noise. Other interpolation techniques, such as using specialised filtering and thresholding to identify the artefact and reconstruct the overlapping M-wave, have been proposed in the past for artefact removal [17], providing promising directions that could be explored in the future. The Gram–Schmidt filtering algorithm [25] is an alternative implementation of adaptive filtering techniques that has been proposed for M-wave removal, which showed the ability to extract vEMG in real-time. Additionally, empirical mode decomposition methods separate the signal into the stationary (i.e., artefact and M-wave) and non-stationary (i.e., vEMG) components for further processing [16,53]; however, they were not assessed in the current study due to the high computational costs, which might be unsuitable for future real-time applications [16].

Some limitations should be acknowledged. Five individuals with no neurological conditions participated in this study. While this is not the typical target population benefitting from FES interventions, the ability of participants to fully control the contraction of their upper-limb muscles was required to assess the performance of the filters in extracting vEMG, which was compared to EMG recorded during the absence of stimulation. To mitigate the lack of ground truth experimental data, we developed a computational model to simulate physiological EMG, enabling unbiased filter assessment. Another limitation is that only the biceps brachii was investigated, and it could be argued that findings may not be transferrable to lower-limb muscles. However, the smaller size of upper-limbs muscles, compared to lower-limbs, may result in increased crosstalk [54]; consequently, fewer challenges should be present when adapting the presented experiments to the lower-limbs. Finally, while this study focused on extracting the vEMG, future endeavours could extend the proposed methodology and analyses to M-wave extraction, e.g., assessment of fatigue during FES [10]. Specifically, improvements to the artefact removal strategy should be considered to ensure that the M-wave is not significantly altered [17].

5. Conclusion

This study presents a comprehensive evaluation of commonly used vEMG extraction methods, first tested through data obtained via a physiological computational model of EMG generation and then experimentally verified. Among the tested methods, the adaptive filter was the most effective method across conditions when no artefact removal was used, however, it required a buffer for the length of one stimulation period, leading to time delays. The adaptive and comb filters were typically the most effective methods across conditions when using blanking or interpolation to replace artefacts, with the comb filter introducing less delay than the adaptive filter, making it more desirable for real-time applications. Overall, we suggest using the described comb filter when developing applications that require the real-time use of vEMG signals extracted from electrically stimulated muscles, while the adaptive filter would be preferred for offline processing or when not using any prior stimulation artefact removal method.

CRediT authorship contribution statement

Matthew J. Hambly: Conceptualization, Methodology, Software, Validation, Writing – original draft, Writing – review & editing, Investigation, Formal analysis, Data curation, Visualization. **Ana Carolina C. de Sousa:** Conceptualization, Methodology, Software, Writing – review & editing, Supervision. **Claudio Pizzolato:** Conceptualization, Methodology, Software, Validation, Writing – review & editing, Supervision, Project administration, Funding acquisition.

Declaration of Competing Interest

The authors declare that they have no known competing financial interests or personal relationships that could have appeared to influence the work reported in this paper.

Data availability

Data will be made available on request.

Acknowledgments

This study was supported by the Motor Accident Insurance Commission, Queensland, Australia (BioSpine project) and by a Griffith University Postgraduate Research Scholarship. The authors would like to thank Prof David Lloyd for the stimulating discussions that allowed us to refine our study design and analyses.

References

[1] C.S. Ahuja, et al., Traumatic spinal cord injury, Nat. Rev. Dis. Primers 3 (1) (2017) 1–21.
[2] N. Jiang, D. Falla, A. d'Avella, B. Graimann, D. Farina, Myoelectric control in neurorehabilitation, Crit. Rev. Biomed. Eng. 38(4) (2010).
[3] J.R. de Kroon, M.J. IJzerman, J. Chae, G.J. Lankhorst, G. Zilvold, Relation between stimulation characteristics and clinical outcome in studies using electrical stimulation to improve motor control of the upper extremity in stroke, J. Rehabil. Med. 37 (2) (2005) 65–74.
[4] J. Jonsdottir, et al., Arm rehabilitation in post stroke subjects: a randomized controlled trial on the efficacy of myoelectrically driven FES applied in a task-oriented approach, PLoS One 12 (12) (2017), e0188642.
[5] R. Thorsen et al., Myoelectrically driven functional electrical stimulation may increase motor recovery of upper limb in poststroke subjects: a randomized controlled pilot study, J. Rehabil. Res. Dev. 50(6) (2013).
[6] R. Merletti, D. Farina, Surface Electromyography: Physiology, Engineering, and Applications, John Wiley & Sons, 2016.

[7] C.J. De Luca, Physiology and mathematics of myoelectric signals, IEEE Trans. Biomed. Eng. 6 (1979) 313–325.
[8] R. Merletti, M. Knaflitz, C.J. DeLuca, Electrically evoked myoelectric signals, Crit. Rev. Biomed. Eng. 19 (4) (1992) 293–340 (in eng).
[9] C. Pizzolato et al., Neuromusculoskeletal modeling-based prostheses for recovery after spinal cord injury, Front. Neurorobot. 13 (2019).
[10] T. Schauer, Sensing motion and muscle activity for feedback control of functional electrical stimulation: ten years of experience in Berlin, Annu. Rev. Control. 44 (2017) 355–374.
[11] A.C.C. de Sousa, M. Valtin, A.P. Bó, T. Schauer, Automatic detection of stimulation artifacts to isolate volitional from evoked EMG activity, IFAC-PapersOnLine 51 (27) (2018) 282–287.
[12] D.T. O'Keeffe, G.M. Lyons, A.E. Donnelly, C.A. Byrne, Stimulus artifact removal using a software-based two-stage peak detection algorithm, J. Neurosci. Methods 109 (2) (2001) 137–145.
[13] C. Frigo, M. Ferrarin, W. Frasson, E. Pavan, R. Thorsen, EMG signals detection and processing for on-line control of functional electrical stimulation, J. Electromyogr. Kinesiol. 10 (5) (2000) 351–360.
[14] E. Ambrosini, et al., A myocontrolled neuroprosthesis integrated with a passive exoskeleton to support upper limb activities, J. Electromyogr. Kinesiol. 24 (2) (2014) 307–317.
[15] T. Schauer, T. Seel, N. Bunt, P. Müller, J. Moreno, Realtime EMG analysis for transcutaneous electrical stimulation assisted gait training in stroke patients, IFAC-PapersOnLine 49 (32) (2016) 183–187.
[16] Y. Zhou, et al., A data-driven volitional EMG extraction algorithm during functional electrical stimulation with time variant parameters, IEEE Trans. Neural Syst. Rehabil. Eng. 28 (5) (2020) 1069–1080.
[17] J. Liu, S. Li, X. Li, C. Klein, W.Z. Rymer, P. Zhou, Suppression of stimulus artifact contaminating electrically evoked electromyography, NeuroRehabilitation 34 (2) (2014) 381–389.
[18] Y. Muraoka, Development of an EMG recording device from stimulation electrodes for functional electrical stimulation, Front. Med. Biol. Eng.: Int. J. Jpn. Soc. Med. Electron. Biol. Eng. 11 (4) (2002) 323–333.
[19] C. Klauer, et al., A patient-controlled functional electrical stimulation system for arm weight relief, Med. Eng. Phys. 38 (11) (2016) 1232–1243.
[20] B.A. Osuagwu, E. Whicher, R. Shirley, Active proportional electromyogram controlled functional electrical stimulation system, Sci. Rep. 10 (1) (2020) 1–15.
[21] S. Sennels, F. Biering-Sorensen, O.T. Andersen, S.D. Hansen, Functional neuromuscular stimulation controlled by surface electromyographic signals produced by volitional activation of the same muscle: adaptive removal of the muscle response from the recorded EMG-signal, IEEE Trans. Rehabil. Eng. 5 (2) (1997) 195–206.
[22] D. Zhang, W.T. Ang, Reciprocal EMG controlled FES for pathological tremor suppression of forearm, in: 2007 29th Annual International Conference of the IEEE Engineering in Medicine and Biology Society, IEEE, 2007, pp. 4810–4813.
[23] K. Gui, H. Yokoi, D. Zhang, Human-FES cooperative control for wrist movement: a preliminary study, Eur. J. Transl. Myol. 26(3) (2016).
[24] E. Langzam, Y. Nemirovsky, E. Isakov, J. Mizrahi, Muscle enhancement using closed-loop electrical stimulation: volitional versus induced torque, J. Electromyogr. Kinesiol. 17 (3) (2007) 275–284.
[25] H. Yeom, Y.-H. Chang, Autogenic EMG-controlled functional electrical stimulation for ankle dorsiflexion control, J. Neurosci. Methods 193 (1) (2010) 118–125.
[26] D. Farina, R. Merletti, A novel approach for precise simulation of the EMG signal detected by surface electrodes, IEEE Trans. Biomed. Eng. 48 (6) (2001) 637–646.
[27] V. Carriou, S. Boudaoud, J. Laforet, F.S. Ayachi, Fast generation model of high density surface EMG signals in a cylindrical conductor volume, Comput. Biol. Med. 74 (2016) 54–68.
[28] D. Farina, A. Blanchietti, M. Pozzo, R. Merletti, M-wave properties during progressive motor unit activation by transcutaneous stimulation, J. Appl. Physiol. 97 (2) (2004) 545–555.
[29] A.N. Burkitt, A review of the integrate-and-fire neuron model: I. Homogeneous synaptic input, Biol. Cybern. 95 (2006) 1–19.
[30] A.H. Caillet, A.T. Phillips, D. Farina, L. Modenese, Estimation of the firing behaviour of a complete motoneuron pool by combining electromyography signal decomposition and realistic motoneuron modelling, PLoS Comput. Biol. 18 (9) (2022), e1010556.
[31] A.H. Caillet, A.T. Phillips, D. Farina, L. Modenese, Mathematical relationships between spinal motoneuron properties, Elife 11 (2022), e76489.
[32] W. Wang, A.D. Stefano, R. Allen, A simulation model of the surface EMG signal for analysis of muscle activity during the gait cycle, Comput. Biol. Med. 36 (6) (2006) 601–618.
[33] P. Rosenfalck, Intra and extracellular fields of active nerve and muscle fibers, A physico (1959).
[34] J. MacDougall, D. Sale, S. Alway, J. Sutton, Muscle fiber number in biceps brachii in bodybuilders and control subjects, J. Appl. Physiol. 57 (5) (1984) 1399–1403.
[35] H.J. Hermens, et al., European recommendations for surface electromyography, Roessingh Res. Dev. 8 (2) (1999) 13–54.
[36] HASOMED, FES Cycling with RehaMove Frequently Asked Questions, https://enableme.com/wp-content/uploads/2015/12/RehaMove_FAQ_Englisch_2014_03.pdf (accessed December 22, 2021).
[37] A. Seth, et al., OpenSim: simulating musculoskeletal dynamics and neuromuscular control to study human and animal movement, PLoS Comput. Biol. 14 (7) (2018), e1006223.
[38] K.R. Holzbaur, W.M. Murray, S.L. Delp, A model of the upper extremity for simulating musculoskeletal surgery and analyzing neuromuscular control, Ann. Biomed. Eng. 33 (6) (2005) 829–840.
[39] C.J. De Luca, M. Knaflitz, Surface Electromyography: What's New? CLUT, 1992.
[40] C. Ma, C. Lin, O.W. Samuel, L. Xu, G. Li, Continuous estimation of upper limb joint angle from sEMG signals based on SCA-LSTM deep learning approach, Biomed. Signal Process. Control 61 (2020), 102024.
[41] S. Sudarsan, E.C. Sekaran, Design and development of EMG controlled prosthetics limb, Proc. Eng. 38 (2012) 3547–3551.
[42] N. Assila, C. Pizzolato, R. Martinez, D.G. Lloyd, M. Begon, EMG-assisted algorithm to account for shoulder muscles co-contraction in overhead manual handling, Appl. Sci. 10 (10) (2020), 3522.
[43] M.F. Rabbi, C. Pizzolato, D.G. Lloyd, C.P. Carty, D. Devaprakash, L.E. Diamond, Non-negative matrix factorisation is the most appropriate method for extraction of muscle synergies in walking and running, Sci. Rep. 10 (1) (2020) 1–11.
[44] P. Mishra, C.M. Pandey, U. Singh, A. Gupta, C. Sahu, A. Keshri, Descriptive statistics and normality tests for statistical data, Ann. Cardiac Anaesthesia 22 (1) (2019) 67.
[45] W. Rong, et al., A Neuromuscular Electrical Stimulation (NMES) and robot hybrid system for multi-joint coordinated upper limb rehabilitation after stroke, J. Neuroeng. Rehabil. 14 (1) (2017) 1–13.
[46] C. Pizzolato, et al., Non-invasive approaches to functional recovery after spinal cord injury: therapeutic targets and multimodal device interventions, Exp. Neurol. 339 (2021), 113612.
[47] J.G. Proakis, Digital Signal Processing: Principles, Algorithms, and Applications, 4/E, Pearson Education India, 2007.
[48] B.C. Garai, P. Das, A.K. Mishra, Group delay reduction in FIR digital filters, Signal Process. 91 (8) (2011) 1812–1825.
[49] N. Lotti, et al., Adaptive model-based myoelectric control for a soft wearable arm exosuit: a new generation of wearable robot control, IEEE Rob. Autom. Mag. 27 (1) (2020) 43–53.
[50] C. Pizzolato, M. Reggiani, D.J. Saxby, E. Ceseracciu, L. Modenese, D.G. Lloyd, Biofeedback for gait retraining based on real-time estimation of tibiofemoral joint contact forces, IEEE Trans. Neural Syst. Rehabil. Eng. 25 (9) (2017) 1612–1621.
[51] K. Manal, W. Rose, A general solution for the time delay introduced by a low-pass Butterworth digital filter: an application to musculoskeletal modeling, J. Biomech. 40 (3) (2007) 678–681.
[52] C. Pizzolato, M. Reggiani, L. Modenese, D. Lloyd, Real-time inverse kinematics and inverse dynamics for lower limb applications using OpenSim, Comput. Methods Biomech. Biomed. Eng. 20 (4) (2017) 436–445.
[53] R. Pilkar, et al., Application of empirical mode decomposition combined with notch filtering for interpretation of surface electromyograms during functional electrical stimulation, IEEE Trans. Neural Syst. Rehabil. Eng. 25 (8) (2017) 1268–1277.
[54] A.P.L. Bo, L.O. da Fonseca, A.C.C. de Sousa, FES-induced co-activation of antagonist muscles for upper limb control and disturbance rejection, Med. Eng. Phys. 38 (11) (2016) 1176–1184.